Journal of Solid State Chemistry 181 (2008) 2845–2851

Contents lists available at ScienceDirect

Journal of Solid State Chemistry

journal homepage: www.elsevier.com/locate/jssc

Solid-state synthesis, characterization and luminescent properties of Eu^{3+}-doped gadolinium tungstate and molybdate phosphors: $Gd_{(2-x)}MO_6:Eu_x^{3+}$ (M = W, Mo)

Fang Lei [a], Bing Yan [a,*], Hao-Hong Chen [b]

[a] Department of Chemistry, Tongji University, Siping Road 1239, Shanghai 200092, China
[b] State Key Laboratory of High Performance Ceramics and Superfine Microstructure, Shanghai Institute of Ceramics, Chinese Academy of Sciences, Shanghai 200050, China

ARTICLE INFO

Article history:
Received 8 April 2008
Received in revised form
9 July 2008
Accepted 10 July 2008
Available online 16 July 2008

Keywords:
Gadolinium tungstate
Gadolinium molybdate
Red phosphor
Luminescent property
Solid-state synthesis

ABSTRACT

Red phosphors gadolinium tungstate and molybdate with the formula $Gd_{(2-x)}MO_6:Eu_x^{3+}$ (M = Mo, W) were successfully synthesized by the solid-state reaction at 900 and 1300 °C for 4 h, respectively. The products were characterized by an X-ray powder diffractometer (XRD), TG–DSC, FT-IR, PL, UV–vis and SEM. Room-temperature photoluminescence indicated that the as-prepared $Gd_{(2-x)}MO_6:Eu_x^{3+}$ (M = Mo, W) had a strong red emission, which is due to the characteristic transitions of Eu^{3+} ($^5D_0 \rightarrow {}^7F_J$, J = 0, 1, 2, 3, 4) for these phosphors. Meanwhile, the $^5D_0 \rightarrow {}^7F_2$ is in the dominant position. The emission quantum efficiency of Eu^{3+} in the $Gd_{(2-x)}MO_6:Eu_x^{3+}$ (M = Mo, W) system has been investigated. The XRD results indicate that both Gd_2WO_6 and Gd_2MoO_6 belong to the monoclinic system with space group $C2/c$ [A. Bril, G. Blasse, J. Chem. Phys. 45 (1966) 2350–2356] and $I2/a$ [A. Bril, G. Blasse, J. Chem. Phys. 45 (1966) 2350–2356], respectively. SEM images indicate that the shape of $Gd_{1.96}WO_6:Eu_{0.04}^{3+}$ is aggregated small particles with a mean diameter of about 300 nm, and the shape of $Gd_{1.96}MoO_6:Eu_{0.04}^{3+}$ is block-like structures.

1. Introduction

With the development of high-resolution devices such as cathode-ray tubes, plasma display panel, field emission displays), high-definition projection television and light-emitting diodes, high-quality phosphors are needed urgently. High quantum efficiency, effective excitation and absorption properties, suitable color purity, and low cost, as well as better morphology and small size are important factors for excellent phosphors [1]. Inorganic phosphors have been extensively investigated for their luminescent properties. As important materials in optical field, rare-earth tungstate and molybdate are two families as the hosts of phosphors that have promising applications in the field of phosphors, optical fibers, scintillators, laser host material and so on [2–7], such as $CaWO_4$ [8], $CaMoO_4$ [9], $PbWO_4$ [10] and $ZnWO_4$ [11] for their superior luminescence properties.

Gadolinium tungstate and molybdate Gd_2MO_6 (M = Mo, W) have attracted much interest for their remarkable properties such as ferroelectricity, laser hosts, phosphors and catalysis [12]. Eu^{3+} as one of the rare-earth ions has been extensively used as active ions of red phosphors for several reasons: (a) the characteristic emission bands at ~613 nm in the red region, and (b) Eu^{3+} can be used as a probe to detect the crystal symmetry [13]. Eu^{3+}-doped gadolinium tungstate and molybdates are known as promising host materials for display applications.

Compared with many studies on metal tungstate and molybdate, rare-earth tungstate and molybdate phosphors have been less studied. Materials belonging to the tungstate and molybdate families have a long history of practical application and have been the object of extensive research over the past century [13].

We synthesized the phosphors of stoichiometric gadolinium tungstate and molybdate doped with Eu^{3+} (Gd_2MO_6 (M = Mo, W)), which were prepared according to a conventional solid-state reaction method using Gd_2O_3 (99.99%), WO_3 (A.R.), MoO_3 (A.R.) and Eu_2O_3 (99.99%) as the starting materials. The aim of this work is to investigate their crystal structures and photoluminescence properties.

2. Experimental section

Starting materials were Gd_2O_3 (99.99%), WO_3 (A.R.), MoO_3 (A.R.) and Eu_2O_3 (99.99%). Stoichiometric raw materials with the formula of $Gd_{1.94}WO_6:Eu_{0.06}^{3+}$were ground in an agate mortar for about 30 min, then transferred to a corundum crucible and heated at 700, 900, 1100 and 1300 °C for 4 h in air, respectively.

* Corresponding author. Fax: +86 21 65982287.
E-mail address: byan@tongji.edu.cn (B. Yan).

0022-4596/$ - see front matter © 2008 Elsevier Inc. All rights reserved.
doi:10.1016/j.jssc.2008.07.008

$Gd_{1.96}W_{0.5}Mo_{0.5}O_6:Eu^{3+}_{0.04}$ and $Gd_{1.96}MoO_6:Eu^{3+}_{0.04}$ by the same process at 1300 °C for 4 h. Meanwhile, a series of phosphors $Gd_{(2-x)}WO_6:Eu_x^{3+}$ ($x = 0$, 0.08, 0.16, 0.32, 0.50, 0.80, 1.00, 2.00) were prepared at 900 °C for 4 h to investigate the relationship of luminescent intensity and the doping concentration of Eu^{3+}.

A routine phase analysis was conducted with an X-ray powder diffractometer (XRD, Bruker D8 Focus) operating at 40 kV/60 mA, using monochromatized Cu$K\alpha$ radiation. The size and shape of the particles were measured by an environmental scanning electronic microscope (Philip XL-30). FT-IR data were collected with a Perkin-Elmer 2000 FT-IR spectrophotometer, and recorded in the 400–4000 cm^{-1} range using KBr pellets. Thermogravimetric analysis was performed on an STA-409PC/4/H LUXX TG–DSC instrument at a heating rate of 10 K/min to a maximum temperature of 1573 K. Photoluminescence spectra were examined using a fluorescence spectrophotometer (SHIMADZU, RF-5301PC) with a Xe lamp at room temperature (RT). UV–vis diffuse reflectance spectra (UV–vis DRS) of the samples were obtained for dry pressed disk samples using a UV–vis spectrophotometer (Lambda-900, Perkin-Elmer). $BaSO_4$ was used as a reference standard. The photoluminescent lifetime was recorded on a single photon counting spectrometer from Edinburgh Instrument (FLS920) with a hydrogen-filled pulse lamp as the excitation source. The data were analyzed by iterative convolution of the luminescence decay profile with the instrument response function using the software package provided by Edinburgh Instruments.

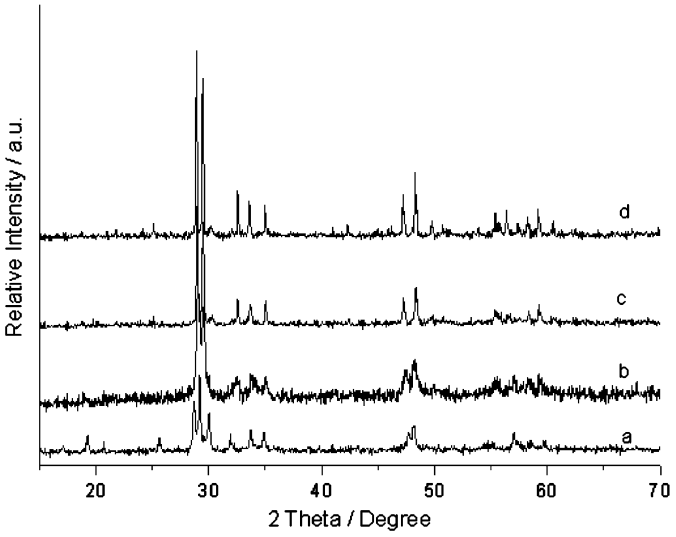

Fig. 1. XRD patterns of $Gd_2WO_6:Eu^{3+}$ synthesized by solid-state reaction at (a) 700 °C, (b) 900 °C, (c) 1100 °C and (d) 1300 °C.

3. Result and discussion

Fig. 1 shows the X-ray diffraction patterns of $Gd_{1.94}WO_6:Eu^{3+}_{0.06}$ powders obtained by solid-state reaction calcined at different temperatures for 4 h: (a) 700, (b) 900, (c) 1100 and (d) 1300 °C. The products obtained at 700 °C contain two phases: $Gd_2(WO_4)_3$ (JCPDS 23-1076) and Gd_2WO_6 (JCPDS 78-1704). The diffraction peaks of (b)–(d) can be indexed to the Gd_2WO_6 phase with space group $C2/c$ [15], which corresponds to JCPDS card no. 78-1704 with lattice parameters of $a = 16.380$, $b = 11.159$ and $c = 5.420$. No impurity peaks were detected in the experimental range. That is, we can obtain pure monoclinic Gd_2WO_6 at 900 °C. The XRD patterns at different calcined temperature indicate that with increase in temperature, the broad diffraction peak became sharper gradually. The strong and sharp diffraction peaks (Fig. 1d) indicate the good crystallization of Gd_2WO_6.

The size and shape of the as-prepared products were measured by SEM. Figs. 2(a) and (b) show the SEM images of the product calcined at 900 °C for 4 h. From the low magnification times of Fig. 2(a), we can observe the whole shape of the as-synthesized products. Several blocks were composed of loosely aggregated nano-particles. Fig. 2(b) shows one of the magnification images; we can observe that Gd_2WO_6 microstructures were composed of small particles with a diameter of about 300 nm, and the particles aggregated. Figs. 2(c) and (d) are the SEM images of Gd_2MoO_6 synthesized at 1300 °C for 4 h with different magnification times.

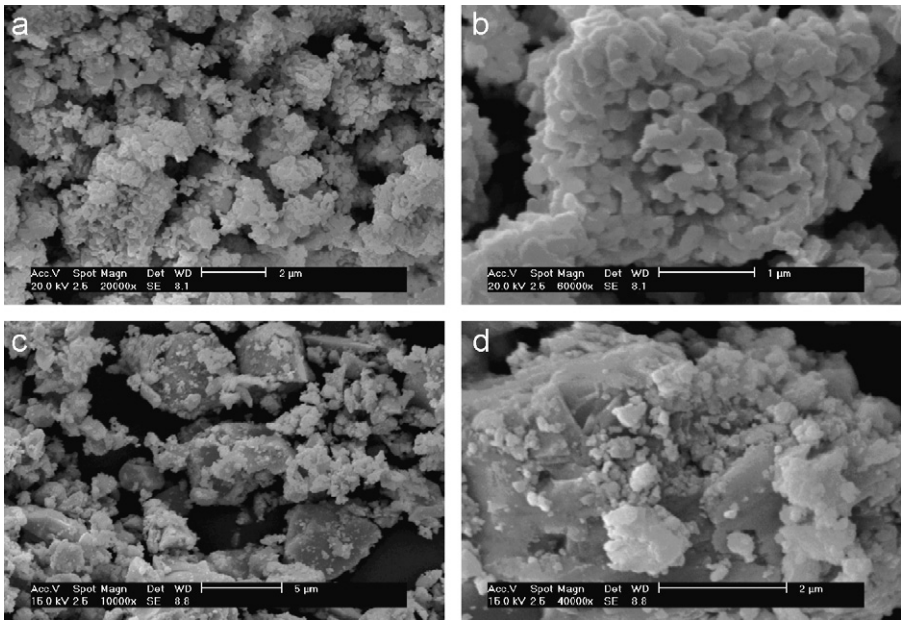

Fig. 2. (a) SEM image of $Gd_{1.96}WO_6:Eu^{3+}_{0.04}$ synthesized by solid-state reaction at 900 °C for 4 h with the magnification time of 20,000, (b) is the same as (a) being magnified at 60,000 times, (c) SEM image of $Gd_{1.96}MoO_6:Eu^{3+}_{0.04}$ synthesized by solid-state reaction at 1300 °C for 4 h with the magnification time of 10,000 and (d) SEM image of $Gd_{1.96}MoO_6:Eu^{3+}_{0.04}$ synthesized by solid-state reaction at 1300 °C for 4 h with the magnification times of 40,000.

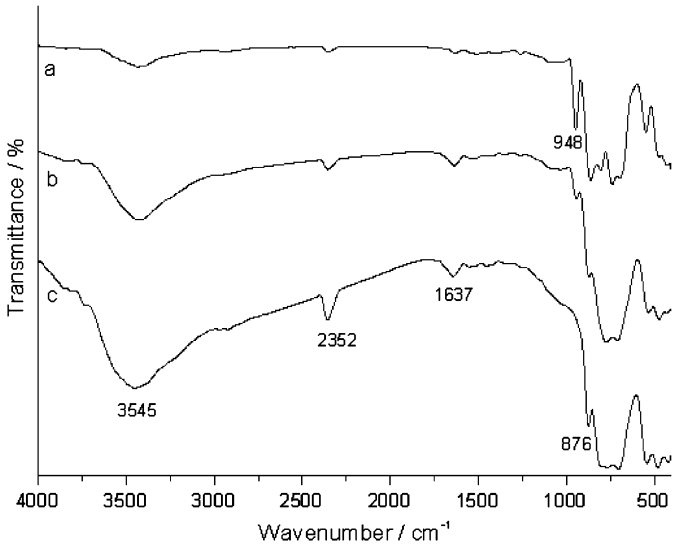

Fig. 3. FT-IR of $Gd_{1.96}WO_6:Eu^{3+}_{0.04}$ phosphor synthesized by solid state at different temperature for 4 h (a) 700, (b) 900 and (c) 1300 °C.

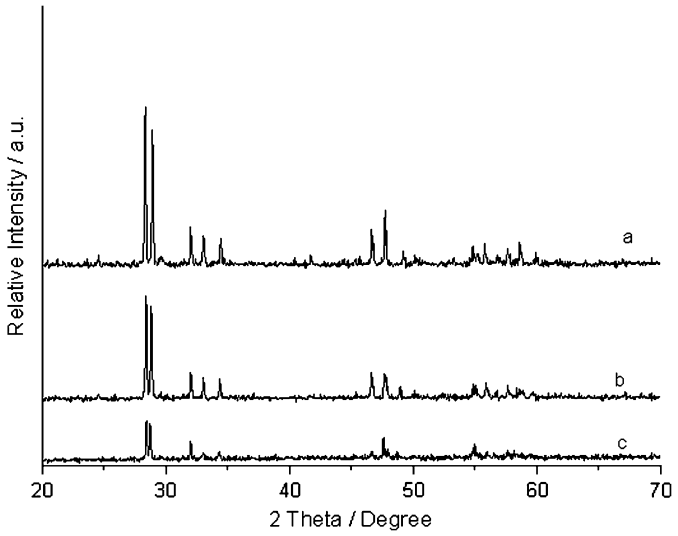

Fig. 4. XRD patterns of (a) $Gd_{1.96}WO_6:Eu^{3+}_{0.04}$, (b) $Gd_{1.96}W_{0.5}Mo_{0.5}O_6:Eu^{3+}_{0.04}$ and (c) $Gd_{1.96}MoO_6:Eu^{3+}_{0.04}$ synthesized by solid-state reaction at 1300 °C for 4 h.

The shape of Gd_2MoO_6 is block-like structures with the diameter at ~5 μm, and some small particles attached on the surface of the blocks can be observed. Its size is larger than that of Gd_2WO_6, which can be attributed to the higher calcinated temperature.

Fig. 3 shows the FT-IR spectrum of $Gd_2WO_6:Eu^{3+}$ powders obtained by solid-state reaction at different calcination temperatures: (a) 700, (b) 900 and (c) 1300 °C. The bands at 3454 and 1637 cm^{-1} are assigned to the O–H stretching vibration and the H–O–H bending vibration of physical absorption water. The band at 2352 cm^{-1} in Figs. 3(a)–(c) is ascribed to the C–O vibration of CO_2 in air. The band at ~876 cm^{-1} can be assigned to the stretching mode of W–O bonds in joint WO_6 octahedra [14]. The FT-IR spectra of Figs. 3(b) and (c) have nearly the same vibration bands, because the products obtained at 900 and 1300 °C are of the same phase $Gd_2WO_6:Eu^{3+}$ with different crystallization. The band ranging from 881 to 675 cm^{-1} has an obvious split in Fig. 3(a), which corresponds to the W–O vibration in the $[WO_4]^{2-}$ and $[WO_6]^{6-}$ groups, respectively.

Fig. 4 shows the XRD patterns of (a) $Gd_{1.96}WO_6:Eu^{3+}_{0.04}$, (b) $Gd_{1.96}W_{0.5}Mo_{0.5}O_6:Eu^{3+}_{0.04}$ and (c) $Gd_{1.96}MoO_6:Eu^{3+}_{0.04}$ synthesized by solid-state reaction at 1300 °C for 4 h. Fig. 4(a) is the XRD pattern of the Gd_2WO_6 phase with space group $C2/c$ [15], which corresponds to JCPDS card no. 78-1704 ($a = 16.380$, $b = 11.159$, $c = 5.420$). Monoclinic $Gd_{1.96}MoO_6:Eu^{3+}_{0.04}$ (Fig. 4c) belongs to the $I2/a$ [15] space group with the lattice parameters of $a = 15.670$, $b = 11.160$ and $c = 5.419$ (JCPDS card no. 24-0423). The molybdate Gd_2MoO_6 is isomorphous with Gd_2WO_6 [15]. The diffraction intensity of the $Gd_{1.96}W_{0.5}Mo_{0.5}O_6:Eu^{3+}_{0.04}$ (Fig. 4(b)) is between $Gd_{1.96}WO_6:Eu^{3+}_{0.04}$ and $Gd_{1.96}MoO_6:Eu^{3+}_{0.04}$. The diffraction intensity depends on the position and the variety of atoms in the crystal lattice. $[MoO_6]$ and $[WO_6]$ both have an octahedron structure, and for the lanthanide contraction, the ionic radius of Mo^{6+} is 0.59 Å and for W^{6+} it is 0.60 Å; there is not much difference between them.

TG–DSC curves for the material of (a) $Gd_{1.96}WO_6:Eu^{3+}_{0.04}$ and (b) $Gd_{1.96}MoO_6:Eu^{3+}_{0.04}$ are shown in Figs.. 5(a) and (b), respectively. The temperature measurement ranges from 40 to 1300 °C. The raw materials were Gd_2O_3, WO_3, MoO_3 and Eu_2O_3. The chemical reaction formula of these two reactions is as follows:

$$0.98\ Gd_2O_3 + WO_3 + 0.02\ Eu_2O_3 \rightarrow Gd_{1.96}WO_6 : Eu_{0.04}{}^{3+} \quad (1)$$

$$0.98\ Gd_2O_3 + MoO_3 + 0.02\ Eu_2O_3 \rightarrow Gd_{1.96}MoO_6 : Eu_{0.04}{}^{3+} \quad (2)$$

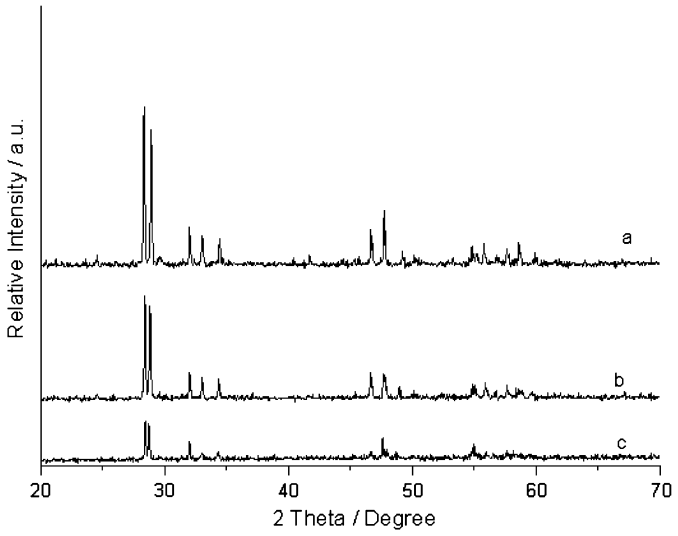

Fig. 5. TG–DSC curve of (a) $Gd_{1.96}WO_6:Eu^{3+}_{0.04}$ and (b) $Gd_{1.96}MoO_6:Eu^{3+}_{0.04}$.

Theoretically, these two reactions have no weight lost. The TG curves (Figs. 5(a) and (b)) of the two phosphors obtained were nearly one line and agreed with the theoretical result. On the DSC curve (Fig. 5(a)), there is an exothermic peak at ~835 °C, which implies that stable crystal phase $Gd_{1.96}WO_6$ forms at this temperature, and the result agrees well with the result of the XRD pattern we had discussed. For the $Gd_{1.96}MoO_6:Eu^{3+}_{0.04}$ phosphors (Fig. 5(b)), there is an endothermic band peaking at 1265 °C on its DSC curve (Fig. 5(b)), which corresponds to the formation of the Gd_2MoO_6 phase.

Figs. 6(a)–(c) show the FT-IR spectra of (a) $Gd_{1.96}WO_6:Eu^{3+}_{0.04}$, (b) $Gd_{1.96}W_{0.5}Mo_{0.5}O_6:Eu^{3+}_{0.04}$ and (c) $Gd_{1.96}MoO_6:Eu^{3+}_{0.04}$ synthesized by solid-state reaction at 1300 °C for 4 h. The band at 3454 cm^{-1} is assigned to the O–H stretching mode of physically adsorbed water. The band at 1643 cm^{-1} is the O–H bending mode. In Fig. 6a, the band 800 cm^{-1} is the vibration of WO_4^{2-} groups. The bands at ~870 cm^{-1} in Fig. 6a and the band at ~850 cm^{-1} in Fig. 6b can be assigned to the stretching mode of W–O bonds in joint WO_6 octahedra. IR spectra below 500 cm^{-1} can be due either

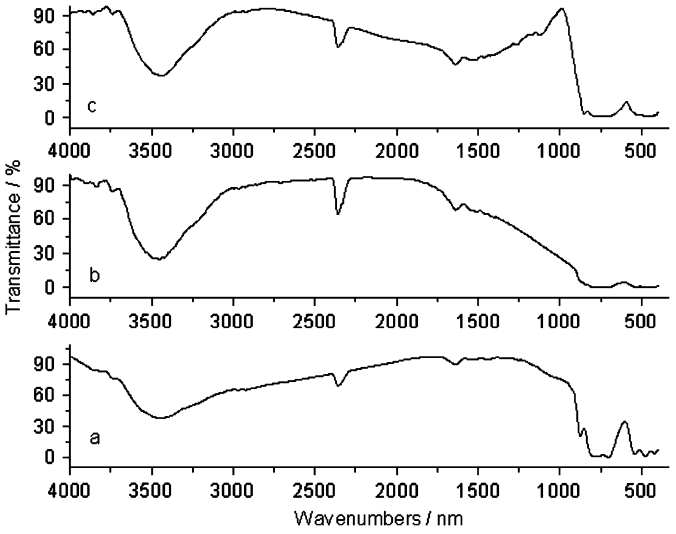

Fig. 6. FT-IR spectra of (a) $Gd_{1.96}WO_6:Eu^{3+}_{0.04}$, (b) $Gd_{1.96}W_{0.5}Mo_{0.5}O_6:Eu^{3+}_{0.04}$ and (c) $Gd_{1.96}MoO_6:Eu^{3+}_{0.04}$ synthesized by solid-state reaction at 1300 °C for 4 h.

to the deformation modes of W–O bonds in WO_6 octahedra or to the deformation modes of W–O–W bridges [13,16]. For $Gd_{1.96}MoO_6$ powders (Fig. 6c), the weak Gd–O at ~550 cm^{-1} and the Mo–O bond (ν_s, 707, 777, 853 cm^{-1}) were also observed [17]. The band at 810 cm^{-1} is assigned to the characteristic absorption band relating to $(MoO_4)^{4-}$. The band at 600 cm^{-1} (w) is related to the Mo–O–Mo bands [18,19].

Fig. 7 shows the UV–vis diffuse reflectance spectra of (a) $Gd_{1.96}WO_6:Eu^{3+}_{0.04}$, (b) $Gd_{1.96}W_{0.5}Mo_{0.5}O_6:Eu^{3+}_{0.04}$ and (c) $Gd_{1.96}MoO_6:Eu^{3+}_{0.04}$ (d) Gd_2WO_6, (e) Gd_2MoO_6 synthesized by solid-state reaction at 1300 °C. These three compounds exhibit a high-intensity broad absorption band in the UV region. We can observe that the absorption band of $Gd_{1.96}WO_6:Eu^{3+}_{0.04}$ ranges from 200 to 350 nm peaking at 293 nm, while the absorption band of $Gd_{1.96}W_{0.5}Mo_{0.5}O_6:Eu^{3+}_{0.04}$ and $Gd_{1.96}MoO_6:Eu^{3+}_{0.04}$ ranges from 200 nm to 450 nm peaking at 375 nm, which corresponds to the O→W and O→Mo ligands to metal charge transfer transition (LMCT), respectively. Besides, some weak sharp peaks appear among the broad absorption bands, which may be due to the structure distortion of the host lattice (tungstate or molybdate), and needs to be further studied deeply. The diffuse reflection spectra of the host compounds Gd_2MoO_6 and Gd_2WO_6 support the assignments of the LMCT. Compared with $Gd_{1.96}WO_6:Eu^{3+}_{0.04}$, the absorption bands of $Gd_{1.96}W_{0.5}Mo_{0.5}O_6:Eu^{3+}_{0.04}$ and $Gd_{1.96}MoO_6:Eu^{3+}_{0.04}$ are much broader than the absorption band of $Gd_{1.96}WO_6:Eu^{3+}_{0.04}$. That is to say, the MoO_6 group has more intense absorption than the WO_6 group in the visible region. The doping of Mo^{6+} is one facile route to extend the absorption band to the visible region for tungstate compounds. The weak bands located at ~610 and 705 nm are ascribed to the *f–f* transition of Eu^{3+}.

The excitation and emission spectra of (a) $Gd_{1.96}WO_6:Eu^{3+}_{0.04}$, (b) $Gd_{1.96}W_{0.5}Mo_{0.5}O_6:Eu^{3+}_{0.04}$ and (c) $Gd_{1.96}MoO_6:Eu^{3+}_{0.04}$ phosphors synthesized by solid-state reaction at 1300 °C are shown in Fig. 8(I) and (II). The excitation spectra were obtained by monitoring the $^5D_0 \rightarrow {}^7F_2$ transition of Eu^{3+} at 613 nm (Fig. 8(I)). The excitation spectra of $Gd_{1.96}WO_6:Eu^{3+}_{0.04}$ show a broadband along with sharp lines of Eu^{3+} at ~359, ~379, ~392 and ~410 nm, which correspond to the transitions of $^7F_0 \rightarrow {}^5D_4$, $^7F_0 \rightarrow {}^5L_7$, $^7F_0 \rightarrow {}^5L_6$ and $^7F_0 \rightarrow {}^5D_2$, respectively (Fig. 8(Ia)). Among the sharp lines, the most intense band is at 392 nm. The intense broadband is noticed in the interval range from 250 to 350 nm with a maximum at ~315 nm ascribed to the charge transfer transition of $O^{2-} \rightarrow W^{6+}$ (LMCT) inside the tungstate group and $O^{2-} \rightarrow Eu^{3+}$ LMCT [13]. The

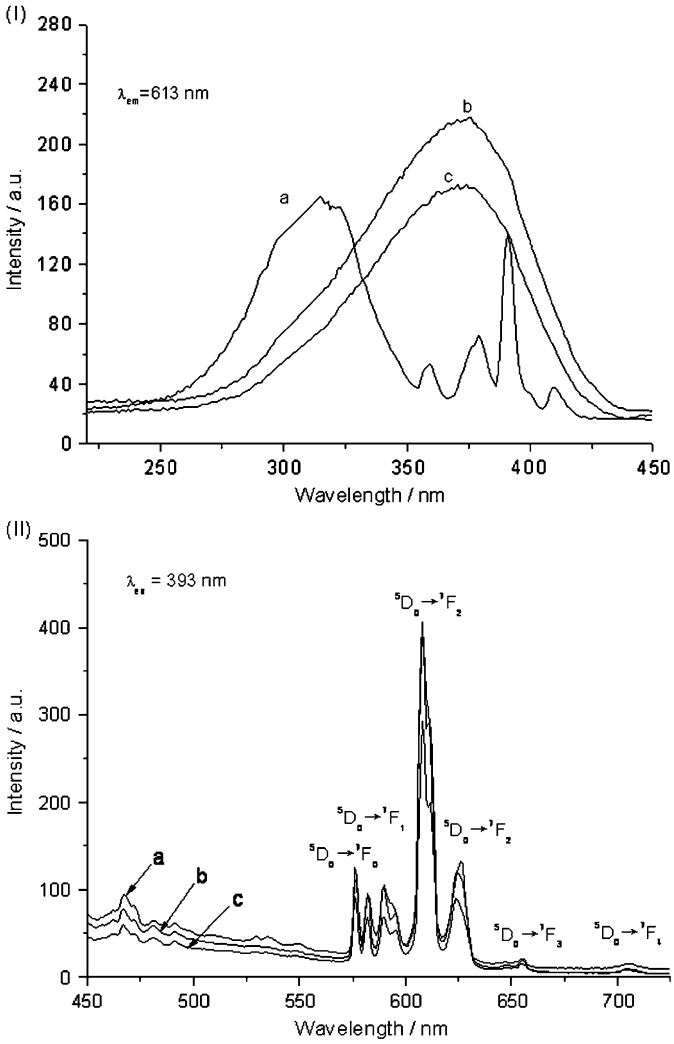

Fig. 7. UV–vis diffuse reflectance spectra of (a) $Gd_{1.96}WO_6:Eu^{3+}_{0.04}$, (b) $Gd_{1.96}W_{0.5}Mo_{0.5}O_6:Eu^{3+}_{0.04}$ and (c) $Gd_{1.96}MoO_6:Eu^{3+}_{0.04}$ (d) Gd_2WO_6, (e) Gd_2MoO_6 synthesized by solid-state reaction at 1300 °C.

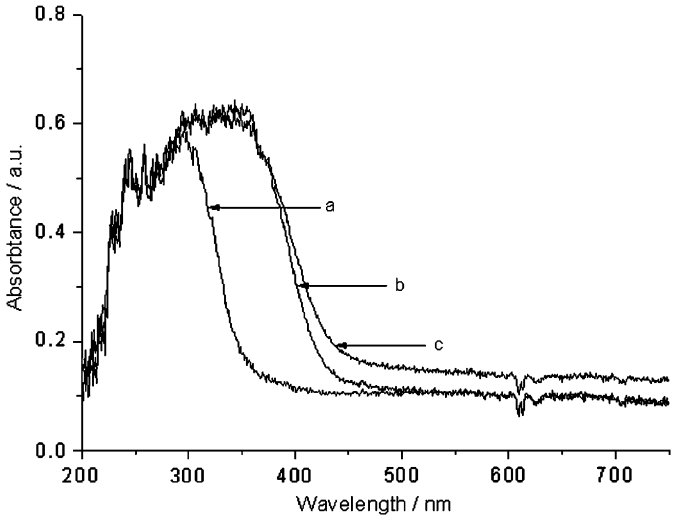

Fig. 8. Excitation (I) and emission (II) spectra of (a) $Gd_{1.96}WO_6:Eu^{3+}_{0.04}$, (b) $Gd_{1.96}W_{0.5}Mo_{0.5}O_6:Eu^{3+}_{0.04}$ and (c) $Gd_{1.96}MoO_6:Eu^{3+}_{0.04}$ synthesized by solid-state reaction at 1300 °C.

presence of the strong band of WO_6^{2-} groups in the excitation spectrum of Eu^{3+} means that there exists an energy transfer from the tungstate groups to Eu^{3+} in $Gd_2WO_6:Eu^{3+}$. The broad excitation bands of $Gd_{1.96}W_{0.5}Mo_{0.5}O_6:Eu^{3+}_{0.04}$ and $Gd_{1.96}MoO_6:Eu^{3+}_{0.04}$ ranging from 250 to 450 nm with a maximum at 375 and 371 nm, respectively, agree well with the diffuse reflectance spectra in Fig. 7, which can be attributed to the charge transfer transition of O^{2-} to Mo^{6+} (LMCT) (Fig. 8(Ib) and (Ic)) [20,21]. The characteristic transition of Eu^{3+} cannot be observed in the excitation spectra of $Gd_{1.96}W_{0.5}Mo_{0.5}O_6:Eu^{3+}_{0.04}$ and $Gd_{1.96}MoO_6:Eu^{3+}_{0.04}$ phosphors, which may be attributed to the overlapping of the broad LMCT band. Fig. 7 shows that $Gd_{1.96}W_{0.5}Mo_{0.5}O_6:Eu^{3+}_{0.04}$ and $Gd_{1.96}MoO_6:Eu^{3+}_{0.04}$ phosphors have absorption bands in the range from 200 to 450 nm.

To compare with the luminescent intensity of these three phosphors and to calculate their luminescent efficiency at the same standard, the emission spectra of $Gd_{1.96}WO_6:Eu^{3+}_{0.04}$, $Gd_{1.96}W_{0.5}Mo_{0.5}O_6:Eu^{3+}_{0.04}$ and $Gd_{1.96}MoO_6:Eu^{3+}_{0.04}$ were all excited under 393 nm (Fig. 8(II)). From the emission spectra, we can observe the characteristic transition of Eu^{3+} ($^5D_0 \rightarrow {}^7F_J$, $J = 0, 1, 2, 3, 4$) in these three phosphors, which correspond to the bands at 576, 582, 589, 595, 607, 611, 626, 655 and 705 nm, respectively. Meanwhile, the $^5D_0 \rightarrow {}^7F_2$ is in the dominant position. This indicates that an energy transfer has occurred from MO_6^{6-} (M = W, Mo) to Eu^{3+} [22]. Eu^{3+} is a good probe for the chemical environment of the rare-earth ion because the $^5D_0 \rightarrow {}^7F_2$ transition (allowed by the electric dipole) is very sensitive to relatively small changes in the surroundings, but the $^5D_0 \rightarrow {}^7F_1$ transition (allowed by magnetic dipole) is insensitive to the environment. In terms of the Judd–Ofelt theory, the magnetic dipole transition is permitted. The electric dipole transition is allowed only in the case when Eu^{3+} occupies a site without an inversion center and is sensitive to local symmetry. Subsequently, when Eu^{3+} ions occupy inversion center sites, the $^5D_0$–$^7F_1$ transitions should be relatively strong, while the $^5D_0$–$^7F_2$ transitions should be relatively weak. The results indicate that Eu^{3+} mainly occupies one site without an inversion center of these three phosphors. A careful analysis of the emission spectra under excitation at 393 nm in Fig. 8(II) reveals the absence of the broadband range from 450 to 550 nm assigned to the O→W LMCT state; this indicates that the tungstate and molybdate groups transfer energy efficiently for the rare-earth ion [21].

In order to investigate the quenching mechanism of the doping concentration of Eu^{3+}, we carried out a series of experiments with the formula of $Gd_{(2-x)}WO_6:Eu_x^{3+}$ ($x = 0, 0.08, 0.16, 0.32, 0.50, 0.80, 1.00, 2.00$) to test the relationship of luminescent intensity and the doping concentration of Eu^{3+}. As can be seen from Fig. 9, all the Eu^{3+}-doped gadolinium tungstate phosphors have five characteristic transitions of $^5D_0 \rightarrow {}^7F_J$ (J = 0–4). With the increase in Eu^{3+} concentration, the luminescent intensity of $^5D_0 \rightarrow {}^7F_2$ (608 nm) reached a maximum at $x = 0.5$. That is, with the increase in the number of luminescent center, the luminescent intensity also increased. When x goes beyond 0.5, the luminescent intensity decreased gradually and reached a minimum at $x = 2$, and concentration quenching takes place. This is because when the doping concentration reaches a certain degree, the distance between Eu^{3+} becomes small, and causes the interactions of the Eu^{3+} ions in the excited state. When $x = 2$, the formula of this phosphor corresponds to the product Eu_2WO_6.

The luminescence decay profiles relative to these three materials could be fitted with single exponentials, from which the RT fluorescence lifetimes were calculated to confirm that all the Eu^{3+} detect the same average environment. Fig. 10 shows the RT luminescence decay curves of the (a) $Gd_{1.96}WO_6:Eu^{3+}_{0.04}$, (b) $Gd_{1.96}W_{0.5}Mo_{0.5}O_6:Eu^{3+}_{0.04}$ and (c) $Gd_{1.96}MoO_6:Eu^{3+}_{0.04}$ ($\lambda_{ex} = 393$ nm, $\lambda_{em} = 613$ nm). The decay profile is well reproduced by a single exponential that reveals a lifetime of 0.695, 0.670 and 0.594 ms, respectively.

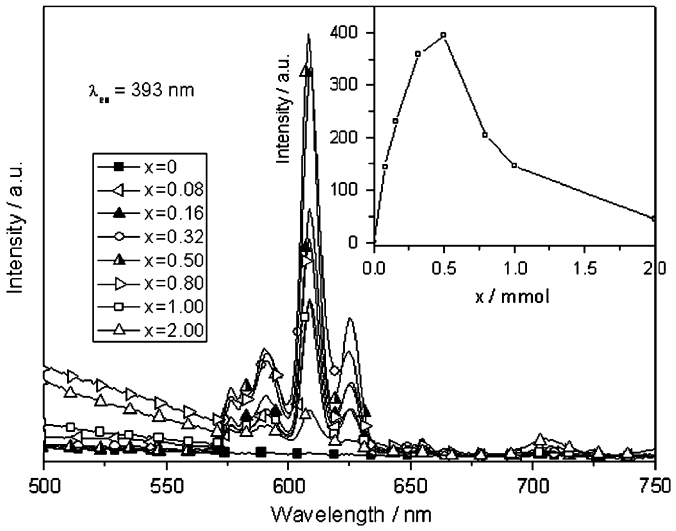

Fig. 9. Emission spectra of $Gd_{(2-x)}WO_6:Eu_x^{3+}$ ($x = 0$, 0.08, 0.16, 0.32, 0.50, 0.80, 1.00, 2.00) synthesized by solid state at 900 °C for 4 h.

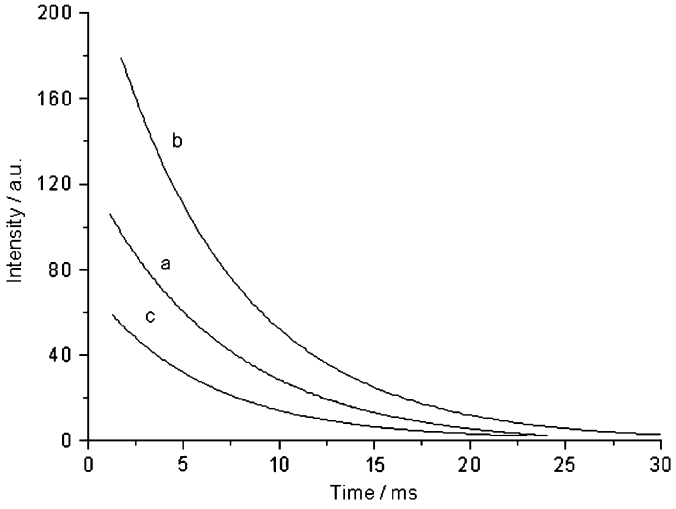

Fig. 10. Room-temperature luminescence decay curves of (a) $Gd_{1.96}WO_6:Eu^{3+}_{0.04}$, (b) $Gd_{1.96}W_{0.5}Mo_{0.5}O_6:Eu^{3+}_{0.04}$ and (c) $Gd_{1.96}MoO_6:Eu^{3+}_{0.04}$ ($\lambda_{ex} = 393$ nm, $\lambda_{em} = 613$ nm).

On the basis of the emission spectra and lifetimes of the $^5D_0$ emitting level, the emission quantum efficiency of the $^5D_0$ europium ion excited state can be determined. The lifetime of the Eu^{3+} first excited state, $\tau_{exp}(^5D_0)$, was detected at 613 nm (the more intense Eu^{3+} emission line) with an excitation wavelength of 393 nm.

We can estimate the efficiency η, of the $^5D_0$ Eu^{3+} excited state. Assuming that only nonradiative and radiative processes are essentially involved in the depopulation of the $^5D_0$ state, η can be defined as follows:

$$\eta = \frac{A_{rad}}{A_{rad} + A_{nrad}}, \quad (1)$$

where A_{rad} and A_{nrad} are the radiative and the nonradiative transition probabilities, respectively.

The emission intensity, I, taken as the integrated intensity S of the emission curves, for the $^5D_0 \rightarrow {}^7F_J$ ($J = 0, 1, 2, 3, 4$) transitions, is expressed by

$$I_{i\rightarrow j} = \hbar w_{i\rightarrow j} A_{i\rightarrow j} N_i \equiv S_{i\rightarrow j}, \quad (2)$$

Table 1
Photoluminescence data of $Gd_{1.96}WO_6:Eu^{3+}_{0.04}$, $Gd_{1.96}W_{0.5}Mo_{0.5}O_6:Eu^{3+}_{0.04}$ and $Gd_{1.96}MoO_6:Eu^{3+}_{0.04}$ phosphors

PL	$Gd_{1.96}WO_6:Eu^{3+}_{0.04}$	$Gd_{1.96}W_{0.5}Mo_{0.5}O_6:Eu^{3+}_{0.04}$	$Gd_{1.96}MoO_6:Eu^{3+}_{0.04}$
λ_{em} (nm)	576, 582, 589, 595, 607, 611, 626, 655, 705		
I_{02}/I_{01}	3.97	4.12	4.45
τ (ms)[b]	0.695	0.670	0.594
$1/\tau$ (s^{-1})	1439	1494	1682
A_{rad} (s^{-1})	656	662	438
A_{nrad} (s^{-1})	783	832	1244
η (%)	45.6	44.3	26.1
Ω_2 (10^{-20})	6.57	6.91	4.98
Ω_4 (10^{-20})	0.39	0.22	0.20

where i and j represent the initial ($^5D_0$) and final levels ($^7F_{0-4}$), respectively, $\hbar w_{i\to j}$ is the transition energy, $A_{i\to j}$ corresponds to Einstein's coefficient of spontaneous emission, and N_i is the population of the $^5D_0$ emitting level [23,24]. The radiative contribution may be calculated from the relative intensities of the $^5D_0\to{}^7F_{0-4}$. The branching ratio for the $^5D_0\to{}^7F_{5,6}$ transitions are not observed experimentally. Therefore, their influence in the depopulation of the $^5D_0$ excited state can be ignored [25,26]. The magnetic dipole $^5D_0\to{}^7F_1$ transition is relatively insensitive to the chemical environments around the Eu^{3+}, and thus can be considered as a reference. The experimental coefficients of spontaneous emission, A_{0J}, were calculated according to the relation as follows:

$$A_{0J} = A_{01}(I_{0J}/I_{01})(\upsilon_{01}/\upsilon_{0J}), \tag{3}$$

where υ_{01} and υ_{0J} are the energy baricenters of the $^5D_0\to{}^7F_1$ and $^5D_0\to{}^7F_J$ transitions, respectively [27]. A_{01} is Einstein's coefficient of spontaneous emission between the $^5D_0$ and $^7F_1$ levels. Since in vacuo, $(A_{0-1})_{vac} = 14.65\,s^{-1}$, when an average index of refraction n equal to 1.506 was considered, the value of $A_{0-1} = n^3(A_{0-1})_{vac} \approx 50\,s^{-1}$ [28–30]. Lifetime, radiative (A_{rad}) and nonradiative (A_{nrad}) transition rates are related through the following equation:

$$A_{tot} = \frac{1}{\tau} = A_{rad} + A_{nrad}, \tag{4}$$

where A_{rad} can be obtained by summing over the radiative rates A_{01} for each $^5D_0\to{}^7F_J$ ($J = 0$–4) transition:

$$A_{rad} = A_{01}\frac{\upsilon_{01}}{I_{01}}\sum_{J=0}^{4}\frac{I_{0J}}{\upsilon_{0J}} = \sum_J A_{0J}, \tag{5}$$

when Eqs. (1)–(5) are applied, the parameters A_{rad} and A_{nrad} and the quantum efficiency values, η, for the $^5D_0$ Eu^{3+} excited state in the five samples can be obtained, as shown in Table 1. The η values of the Eu^{3+} in these three phosphors $Gd_{1.96}WO_6:Eu^{3+}_{0.04}$, $Gd_{1.96}W_{0.5}Mo_{0.5}O_6:Eu^{3+}_{0.04}$ and $Gd_{1.96}MoO_6:Eu^{3+}_{0.04}$ are 45.6%, 44.3% and 26.1%, respectively. That is, the luminescent quantum efficiency of $Gd_{1.96}WO_6:Eu^{3+}_{0.04}$ is higher than that of $Gd_{1.96}W_{0.5}Mo_{0.5}O_6:Eu^{3+}_{0.04}$ and $Gd_{1.96}MoO_6:Eu^{3+}_{0.04}$ gradually. In spite of the slight difference in ratio of red and orange from each other, the lifetime of $Gd_{1.96}WO_6:Eu^{3+}_{0.04}$ is much higher than the other two phosphors, especially the $Gd_{1.96}MoO_6:Eu^{3+}_{0.04}$ phosphor.

From the emission spectra of the Eu^{3+} (Fig. 7(II)) we have determined the experimental intensity parameters Ω_2 and Ω_4 using the $^5D_0\to{}^7F_2$ and $^5D_0\to{}^7F_4$ transitions, and they are estimated according to the equation [13,23,24,27,31]

$$A_{0-\lambda} = \frac{4e^2\omega^3}{3\hbar c^3}\frac{1}{2J+1}\chi\sum_\lambda \Omega_\lambda\left\langle {}^5D_0\middle\|U^{(\lambda)}\middle\|{}^7F_J\right\rangle^2, \tag{6}$$

where $A_{0-\lambda}$ is the coefficient of spontaneous emission, e the electronic charge, ω the angular frequency of the transition, $\hbar$ Planck's constant over 2π, c the velocity of light, χ the Lorentz local field correction that is given by $n(n^2+2)^2/9$ with the refraction index $n = 1.5$ [23], and $\langle {}^5D_0||U^{(\lambda)}||{}^7F_J\rangle^2$ values are the square reduced matrix elements whose values are 0.0032 and 0.0023 for $J = 2$ and 4 [32], respectively. The Ω_6 parameter was not determined since the $^5D_0\to{}^7F_6$ transition could not be experimentally detected. The Ω_2 and Ω_4 intensity parameters for the three phosphors are shown in Table 1. Ω_2 of $Gd_{1.96}WO_6:Eu^{3+}_{0.04}$ (6.57×10^{-20}) is higher than that of $Gd_{1.96}MoO_6:Eu^{3+}_{0.04}$ (4.98×10^{-20}), suggesting that the Eu^{3+} ion is located in a more polarizable chemical environment in Gd_2WO_6 than in Gd_2MoO_6. It means that Gd_2WO_6 possesses a stronger covalency than Gd_2MoO_6. The radium of W^{6+} is similar to that of Mo^{6+} for the lanthanide contraction effect, while the interaction between W–O is stronger than that of Mo–O for the more electronic layer.

4. Conclusion

In summary, red phosphors of $Gd_{(2-x)}MO_6:Eu_x^{3+}$ (M = Mo, W) have been successfully synthesized by solid-state reaction at 900–1300 °C for 4 h. The XRD results show that all samples are monoclinic phase. The molybdate Gd_2MoO_6 is isomorphous with Gd_2WO_6. The samples $Gd_{(2-x)}MO_6:Eu_x^{3+}$ (M = Mo, W) can be excited efficiently by UV (393 nm) and emit red light at ~608 nm. And they both have an intense absorption band in the UV region range from 200 to 350 nm corresponding to the O→W and O→Mo LMCT, respectively. The quantum efficiency of the Eu^{3+} in these three phosphors $Gd_{1.96}WO_6:Eu^{3+}_{0.04}$, $Gd_{1.96}W_{0.5}Mo_{0.5}O_6:Eu^{3+}_{0.04}$ and $Gd_{1.96}MoO_6:Eu^{3+}_{0.04}$ are 45.6%, 44.3% and 26.1%, respectively. In spite of the slight difference in the ratio between red and orange , the lifetime of $Gd_{1.96}WO_6:Eu^{3+}_{0.04}$ is much higher than the other two phosphors, especially the $Gd_{1.96}MoO_6:Eu^{3+}_{0.04}$ phosphor.

Acknowledgment

The authors gratefully acknowledge the financial support for this research from the National Nature Science Foundation of China (no. 20671072).

References

[1] G.X. Liu, G.Y. Hong, J.X. Wang, X.T. Dong, J. Alloys Compds. 432 (2007) 200–204.
[2] Q. Gong, X.F. Qian, X.D. Ma, Z.K. Zhu, Cryst. Growth Des. 6 (2006) 1821–1825.
[3] Q.T. Takagi, K. Fukazawa, Appl. Phys. Lett. 36 (1980) 278–279.
[4] H. Wang, F. Medina, D. Liu, Y. Zhou, Q. Zhang, Phys. Rev. B 45 (1992) 10356–10362.
[5] K. Tanaka, T. Miyajima, N. Shirai, Q. Zhang, R. Nakata, J. Appl. Phys. 77 (1995) 6581–6587.
[6] H.W. Liao, Y.F. Wang, X.M. Liu, Y.D. Li, Y.T. Qian, Chem. Mater. 12 (2000) 2819–2821.
[7] S. Kwan, F. Kim, J. Akana, P.D. Yang, Chem. Commun. 5 (2001) 447–448.
[8] Q. Zhang, W.T. Yao, X.Y. Chen, L.W. Zhu, Y.B. Fu, G.B. Zhang, L.S. Sheng, S.H. Yu, Cryst. Growth Des. 7 (2007) 1423–1431.
[9] G. Ahmad, M.B. Dickerson, B.C. Church, Y. Cai, S.E. Jones, R.R. Naik, J.S. King, C.J. Summers, N. Kröger, K.H. Sandhage, Adv. Mater. 18 (2006) 1759–1763.
[10] Z.J. Yi, T.Y. Liu, Q.R. Zhang, Y.Y. Sun, Phys. Status Solidi B 243 (2006) 1802–1807.
[11] Q.L. Dai, H.W. Song, X. Bai, G.H. Pan, S.Z. Lu, T. Wang, X.G. Ren, H.F. Zhao, J. Phys. Chem. C 111 (2007) 7586–7592.
[12] H. Naruke, T. Yamase, Inorg. Chem. 41 (2002) 6514–6520.
[13] C.A. Kodaira, H.F. Brito, M.C.F.C. Felinto, J. Solid State Chem. 171 (2003) 401–407.
[14] E. Tomaszewicz, Solid State Sci. 8 (2006) 508–512.
[15] A. Bril, G. Blasse, J. Chem. Phys. 45 (1966) 2350–2356.
[16] E. Tomaszewicz, Thermochim. Acta 447 (2006) 69–74.
[17] G.Z. Li, Z.L. Wang, Z.W. Quan, X.M. Liu, M. Yu, R.S. Wang, J. Lin. Surf. Sci. 600 (2006) 3321–3326.
[18] A. Packter, A. Omono, Cryst. Res. Technol. 19 (1984) 467–476.
[19] V. Hangloo, S. Pandita, K.K. Bamzai, P.N. Kotru, N. Sahni, Cryst. Growth Des. 3 (2003) 753–759.

[20] J.C. Krupa, J. Alloys Compds. 225 (1995) 1–10.
[21] C.A. Kodaira, H.F. Brito, O.L. Malta, O.A. Serra, J. Lumin. 101 (2003) 11–21.
[22] M.L. Pang, X.M. Liu, J. Mater. Res. 20 (2005) 2676–2681.
[23] O.L. Malta, M.A. Couto dos Santos, L.C. Thompson, N.K. Ito, J. Lumin. 69 (1996) 77–84.
[24] O.L. Malta, H.F. Brito, J.F.S. Menezes, F.R. Goncüalves e Silva, S. Alves, F.S. Farias, A.V.M. Andrade, J. Lumin. 75 (1997) 255–268.
[25] P.C.R. Soares-Santos, H.I.S. Nogueira, V. Felix, M.G.B. Drew, R.A.S. Ferreira, L.D. Carlos, T. Trindade, Chem. Mater. 15 (2003) 100–108.
[26] L.D. Carlos, Y. Messaddeq, H.F. Brito, R.A.S. Ferreira, V.D. Bermudez, S.J.L. Ribeiro, Adv. Mater. 12 (2000) 594–598.
[27] E.E.S. Teotonio, J.G.P. Espinola, H.F. Brito, O.L. Malta, S.F. Oliveria, D.L.A. de Foria, C.M.S. Izumi, Polyhedron 21 (2002) 1837–1844.
[28] M.H.V. Werts, R.T.F. Jukes, J.W. Verhoeven, Phys. Chem. Chem. Phys. 4 (2002) 1542–1548.
[29] S.J.L. Ribeiro, K. Dahmouche, C.A. Ribeiro, C.V. Santilli, S.H.J. Pulcinelli, J. Sol–Gel Sci. Technol. 13 (1998) 427–432.
[30] M.F. Hazenkamp, G. Blasse, Chem. Mater. 2 (1990) 105–110.
[31] J.C. Boyer, F. Vetrone, J.A. Capobianco, A. Speghini, M. Bettinelli, J. Phys. Chem. B 108 (2004) 20137–20143.
[32] W.T. Carnall, H. Crosswhite, H.M. Crosswhite, Argonne National Laboratory, Argonne, 1978.